Phase imaging using highly coherent X-rays: radiography, tomography, diffraction topography

José Baruchel,[a]***** **Peter Cloetens,**[a] **Jürgen Härtwig,**[a] **Wolfgang Ludwig,**[a] **Lucia Mancini,**[a]† **Petra Pernot**[a] **and Michel Schlenker**[b]

[a]*ESRF, BP 220, 38043 Grenoble, France, and* [b]*Laboratoire Louis Néel, CNRS, BP 166, 38042 Grenoble, France. E-mail: baruchel@esrf.fr*

Several hard X-rays imaging techniques greatly benefit from the coherence of the beams delivered by the modern synchrotron radiation sources. This is illustrated with examples recorded on the 'long' (145 m) ID19 'imaging' beamline of the ESRF. Phase imaging is directly related to the small angular size of the source as seen from one point of the sample ('effective divergence' $\simeq$ microradians). When using the 'propagation' technique, phase radiography and tomography are instrumentally very simple. They are often used in the 'edge detection' regime, where the jumps of density are clearly observed. The *in situ* damage assessment of micro-heterogeneous materials is one example of the many applications. Recently a more quantitative approach has been developed, which provides a three-dimensional density mapping of the sample ('holotomography'). The combination of diffraction topography and phase-contrast imaging constitutes a powerful tool. The observation of holes of discrete sizes in quasicrystals, and the investigation of poled ferroelectric materials, result from this combination

1. Introduction

The advent of synchrotron radiation facilities with small 'effective divergence' α (small angular size of the source as seen from one point of the sample) made it possible to observe phase images by simple 'propagation' of the beam. This can be performed, for instance, at station 7.6 of the SRS, Daresbury Laboratory, where the effective divergence α is less than 3 µrad (Lang *et al.*, 1987; Tanner *et al.*, 1998). However, the availability of third-generation synchrotron radiation sources has turned this propagation-based form of radiography into a standard experimental technique, in which contrast arises from phase variations across the transmitted beam through Fresnel diffraction (Snigirev *et al.*, 1995; Cloetens *et al.*, 1996). Two forms of this technique are now operational: either the edges of the inhomogeneities are directly imaged, or it is possible to reconstruct quantitatively the phase shift introduced by the object, from images recorded at different distances (Cloetens, Ludwig, Baruchel, Van Dyck *et al.*, 1999). Phase radiography and its three-dimensional companion, phase tomography, are providing new information on the mechanics of composites and polymers (Cloetens, Pateyron-Salomé *et al.*, 1997; Buffière *et al.*, 1999) as well as on biological materials (Spanne *et al.*, 1999). Various works

on coherent X-ray optics have been recently carried out. For instance, the Talbot effect which applies to periodic objects, a classical and spectacular example of Fresnel diffraction (self-imaging, periodic as a function of defocusing distance), was investigated in the hard X-ray range (Cloetens, Guigay *et al.*, 1997), and a Fresnel biprism was built up from two diamond crystals and the corresponding interference patterns were recorded and used to characterize the source (Lang & Makepeace, 1999).

About 40 years ago, Bragg-diffraction imaging (X-ray topography) developed into practical use. It directly reveals crystal defects in the bulk of large single crystals, and helped to produce large practically perfect crystals for the microelectronics industry. An exciting recent development is the combination of phase radiography with X-ray topography. When applied to quasicrystals, information about local strain fields and inhomogeneities such as holes with discrete sizes, or precipitates, is simultaneously obtained (Mancini, Reinier *et al.*, 1998).

The phase effects can also be observed in the diffracted beam image itself. Faint defects can be visualized using the associated phase modulation of the diffracted beam (Baruchel, 1996; Kuznetsov *et al.*, 1999). Spectacular effects also result from the phase contribution to Bragg-diffraction imaging in periodically poled ferroelectric crystals (Hu *et al.*, 1998; Rejmánková-Pernot *et al.*, 1998). The contrast mechanism is now understood to be related to the Talbot

---

† Present address: Instituto LAMEL, CNR, Via Gobetti 101, 40129 Bologna, Italy.

effect, but this time in Bragg diffraction. It mainly originates from the phase shift between the structure factors of oppositely poled regions. A direct measurement of this phase difference is thus obtained from images made at different distances from the sample (Rejmánková-Pernot *et al.*, 1998). This approach, again made possible by the large spatial coherence of the X-ray beam, in turn provides important quantitative information about atom displacements at the microscopic level.

2. Phase radiography and tomography

An X-ray beam transmitted through a sample is usually affected both in its amplitude, through absorption and scattering, and in its phase. The latter can be expressed by

$$\varphi(x, y) = (2\pi/\lambda) \int [n(x, y, z) - 1] \, dz, \qquad (1)$$

with the index of refraction n equal to

$$n = 1 - (r_c \lambda^2/2\pi V) \sum_j \left[Z_j + f'_j(\lambda) \right]. \qquad (2)$$

Here r_c is the classical electron radius ($r_c = 2.8$ fm), Z_j is the atomic number and $f'_j(\lambda)$ is the real part of the dispersion correction to the atomic scattering factor for atom j, the sum being taken over all the atoms contained in volume V. Thus, except near absorption edges, $(n - 1)$ is proportional to the electron density, hence approximately to the mass density along the X-ray path. The distribution of the phase across the beam at the exit of a sample is usually inhomogeneous, and it contains valuable information. However, at this stage it does not affect the intensity, and detecting it normally requires special set-ups.

A way of turning phase variations of the X-ray beam across a specimen into images is to use Bonse–Hart-type interferometry (Bonse & Hart, 1965). The phase image is obtained through interference between the beam transmitted through the sample and a reference beam. Recently this approach has developed into a quantitative three-dimensional imaging technique by Momose and co-workers (Momose *et al.*, 1995) and Bonse and co-workers (Bonse *et al.*, 1998). This method produces maps of the phase shift introduced by the sample. An alternative way of detecting phase effects is X-ray refraction imaging, which uses the high angular sensitivity of double perfect crystal set-ups to record essentially the first derivative of the phase shift. This led to impressive pictures, obtained using laboratory X-rays by several groups (Förster *et al.*, 1980; Somenkov *et al.*, 1991; Ingal & Beliaevskaya, 1995; Davis *et al.*, 1995). This technique was of course extended to synchrotron radiation, under different names, one of them being 'diffraction-enhanced imaging' (Chapman *et al.*, 1998). In optical terms, this last technique corresponds to Schlieren imaging.

We will concentrate in the present paper on a third, instrumentally simple, way of producing phase images: the propagation technique. Preliminary imaging experiments at the ESRF showed that objects with negligible absorption

for the hard X-rays used are imaged with considerable contrast, provided the detector is placed far enough from the specimen. It was soon established that this is basically due to Fresnel diffraction, *i.e.* to simple free-space propagation (Snigirev *et al.*, 1995; Cloetens *et al.*, 1996), and that the image shows the second derivative of the phase shift introduced by the sample. This opens the way for the investigation of materials which exhibit small variations in density, not detectable by usual absorption radiography (Cloetens, Pateyron-Salomé *et al.*, 1997). This is associated with the considerable lateral coherence length $d_c = \lambda/2\alpha$ of the beam, resulting from the small size of the source and its large distance from the specimen (small effective divergence α). For third-generation synchrotron radiation in general, and more particularly on long beamlines (like ID19 at the ESRF), α can be as small as 0.2 µrad, leading to d_c values of up to 0.3 mm.

The formal framework for the description is Fresnel diffraction. The basic effect is the interference of the unaffected part of the beam with diffracted components. The effect is not visible for 'very small' specimen–detector distances L because of the limited spatial resolution of the detector and because of the weakness of the contrast. The conspicuous feature at 'small' L is the delineation of the phase discontinuities, *i.e.* of the edges of the sample, and of sharp boundaries in the sample ('edge detection'). Pictures taken at growing L involve broader and a larger number of detectable fringes. At 'large' L the image loses resemblance to the object, and becomes an in-line hologram. A closer look at the process makes it possible to make the statements 'small' or 'large' quantitative. The relevant factor is the relation between the size a of a feature of the object and the radius of the first Fresnel zone $r_F = (\lambda L)^{1/2}$ in the approximation where the source–specimen distance is very large compared with L. The imaging regime where the image looks like the sample is for $r_F < a$, and the Fraunhofer limit, with the diffraction pattern related to the Fourier transform of the transmitted complex amplitude, is when $a << r_F$.

The Talbot effect (Talbot, 1836) is a classic case of Fresnel diffraction in visible-light optics. It is the self-imaging behaviour, periodic along the mean propagation direction z, with period $z_T = 2p^2/\lambda$, of an object that is periodic along x, with period p. This was investigated in the hard X-ray case, and was found to be a good way of quantitatively determining the spatial coherence of the beam, hence the size of the source (Cloetens, Guigay *et al.*, 1997). A Fresnel biprism was also used to estimate the size of the source (Lang & Makepeace, 1999).

A great deal of effort is being devoted to two further aspects: (i) the use of the direct 'edge detection' approach (including its tomographic extension), for applications which require the improved sensitivity of phase images with respect to the absorption ones, and (ii) the quantitative reconstruction of the phase distribution in the beam and the three-dimensional mapping of the refractive index distribution in the specimen.

Phase tomography, in its 'edge detection' version, is now a standard technique. It shows the volume distribution of sudden variations of the refractive index decrement, proportional to the electron density. It was shown that the standard algorithm of absorption tomography for the three-dimensional reconstruction provides reasonable results for edge detection (Cloetens, Pateyron-Salomé *et al.*, 1997). In this regime, phase tomography was used to produce images of medical objects (Spanne *et al.*, 1999). Let us emphasize that this technique has already produced results which go well beyond the simple demonstration experiments. One example, in materials science, is the investigation of the mechanism of the fracture of silicon-carbide-reinforced aluminium alloys (Cloetens, Pateyron-Salomé *et al.*, 1997; Buffière *et al.*, 1999).

Phase reconstruction (sometimes called holographic reconstruction) for two-dimensional images is based on the combination of several images recorded at different L values. Good results are now obtained with an approach based on methods developed for electron microscopy (Coene *et al.*, 1992). Once the phase maps are obtained through holographic reconstruction (Cloetens, Ludwig, Baruchel, Guigay *et al.*, 1999), there is no conceptual difficulty in bringing together many maps corresponding to different orientations of the sample, and in producing the tomographic three-dimensional reconstruction. This combined procedure was applied to a polystyrene foam: for each of 700 angular positions of the sample, the phase map was retrieved using images recorded at four distances. A tomographic slice with the polymer appearing in black is shown in Fig. 1. The highest accessible spatial frequency is determined by the resolution of the detector. Quantitative phase mapping and tomography are becoming operational, and provide a new approach to the characterization of materials on the micrometer scale (Cloetens, Ludwig, Baruchel, Van Dyck *et al.*, 1999).

Three points should be mentioned at this stage. On one hand, phase radiography is very simple instrumentally, since nothing more than a monochromatic beam with suitable coherence is required. However, it puts stringent demands on the beamline in order to conserve the uniformity of the beam (Espeso *et al.*, 1998). Any inhomogeneity in beryllium windows or filters shows up as spurious contrast on the images even if its effect on the statistically measured coherence of the beam is negligible. Also, the monochromator surface now has to be much cleaner than for regular applications, where it is essential but sufficient that it is strain free. On the other hand, phase reconstruction is not just a luxury for perfectionists. The fringe structure associated with Fresnel diffraction deteriorates the resolution to the Fresnel zone radius, and going beyond this limit requires the determination of the phase distribution. Finally, because third-generation synchrotron sources are not common household items, there has been a search for alternative approaches that can be used in the laboratory. Wilkins *et al.* (1996) have shown that radiographs made using the polychromatic beam from a micro-

focus X-ray generator do reveal the feature that is rather wavelength-independent, *viz.* phase jumps.

3. Combined use of phase radiography/ tomography and diffraction topography

Quasicrystals are non-periodic solids with long-range order. A lot of effort has been devoted, from their discovery in 1984, to understanding their peculiar properties, in particular their growth mechanism and stability. They produce fine diffraction peaks for X-rays just as crystals do. Therefore they are amenable to Bragg-diffraction imaging too. The combination of diffraction topography and phase imaging was important for the actual characterization of the inhomogeneities in high-quality icosahedral Al–Pd–Mn quasicrystals: internal oriented dodecahedral holes with a shape featuring the icosahedral point symmetry of the investigated material, and with sizes exhibiting a discrete distribution, are observed to be present (Mancini, Reinier *et al.*, 1998) within the bulk of all the high-quality Al–Pd–Mn quasicrystals. The size distribution displays peaks at sizes of 22, 5 and slightly more than 1 μm. Simple gas bubbles would lead to a continuous
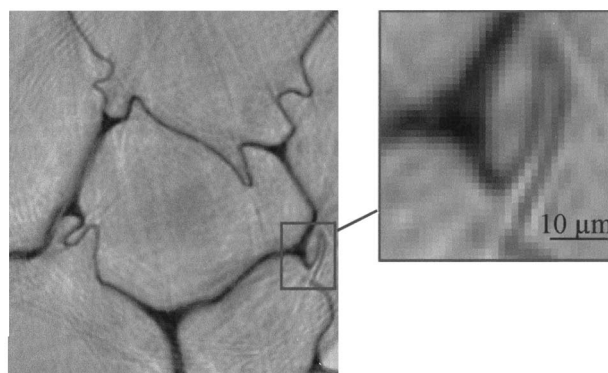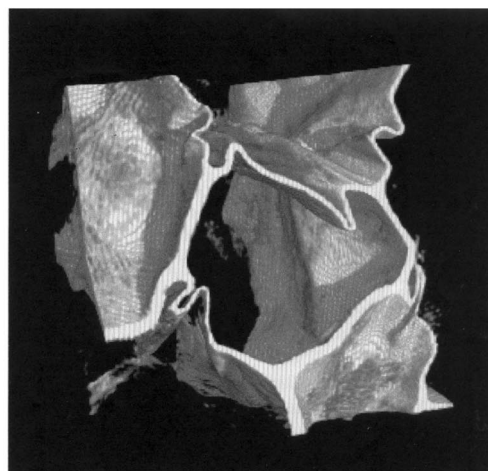

Figure 1
'Holotomographic' reconstruction of a polystyrene foam sample. Slice through the reconstructed volume showing the distribution of the refractive index decrement. X-ray energy: 18 keV.

distribution. The jump from one size to the next corresponds to the factor τ^3, where τ is the golden mean, a basic ingredient in all theoretical approaches of quasicrystals. The three-dimensional reconstruction resulting from phase microtomography shows that the average distance between neighbouring holes is, again, about τ^3 multiplied by the hole size. The observed features are in fair agreement with a geometrical approach which describes the quasicrystal structure in terms of a hierarchical self-similar packing of overlapping atomic clusters, such that an inflation scale factor τ^3 preserves long-range order but generates a hierarchy of holes (Mancini, Janot *et al.*, 1998). Further experiments are being performed to better understand the physical implications of these observations.

Fig. 2 shows a diffraction image ('topograph') and the corresponding phase image. The topograph shows a white–black contrast which indicates that a gradient of distortion is present in the hole neighbourhood. This contrast can be simulated by just assuming, as a first approximation, that the deformation field is similar to the classical one around a spherical inclusion in a crystal.

4. Phase effects in Bragg-diffraction images

Phase effects have long been familiar in standard X-ray diffraction imaging (X-ray topography). Interference between wave-fields, or Bloch waves, within the crystal produce Pendellösung-type fringes (see, for instance, Authier, 1996), which are sensitive indicators of distortion,

and can even yield directly the modulus of the structure factor of the reflection used.

The combination of Bragg and Fresnel diffraction has been successfully achieved ('Bragg–Fresnel lenses') for hard X-ray focusing. More generally, any abrupt variation of thickness of a crystal (surface scratch, for instance) gives rise to a phase image. One of the originalities of the present approach, which uses a highly coherent beam, is that it can reveal a defect even in a case where 'usual' diffraction topography fails to show any contrast, *i.e.* when the diffraction vector is perpendicular to the deformation vector. This type of contrast was recently analysed by Kuznetsov and co-workers (Kuznetsov *et al.*, 1999), who established a simple relationship, valid in some cases, between the phase distribution at the exit surface and the corresponding displacement field within the diffracting crystal.

Another effect was recently observed in several poled ferroelectric crystals ($LiNbO_3$, KTP, KTA) (Hu *et al.*, 1998; Rejmánková-Pernot *et al.*, 1998). The poling process leads to the controlled coexistence of ferroelectric domains, with mutually inverted crystal structure, with width typically in the 10 µm range. Topographs were recorded with the parallel-faced crystal set for Bragg diffraction, in reflection (Bragg geometry) as well as in transmission (Laue geometry); in both cases the scattering plane was parallel to the walls between poled regions, so that X-ray wave-field propagation occurred entirely in a given type of domain. Since the diffracted wave leaving the crystal has the phase
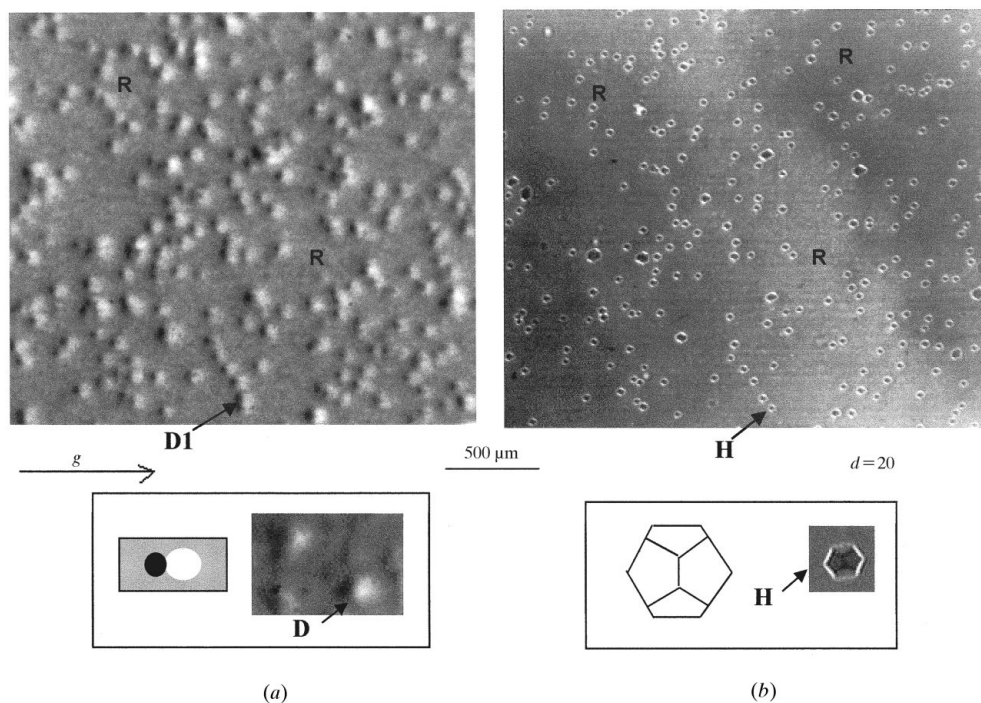

Figure 2
(*a*) Bragg-diffraction image and (*b*) phase image, recorded at $d = 20$ cm, of holes (H) in an icosahedral Al–Pd–Mn quasicrystal. The letters R are aimed to help identify the same region on both images. The diffraction image shows that the presence of a hole is associated with a distortion (D1 in the main figure and D in the magnification) of the quasicrystal in its neighbourhood. g is the projection of the diffraction vector on the image plane.

D = 0.11 m

30 μm

D = 0.30 m

D = 0.60 m

D = 1.09 m
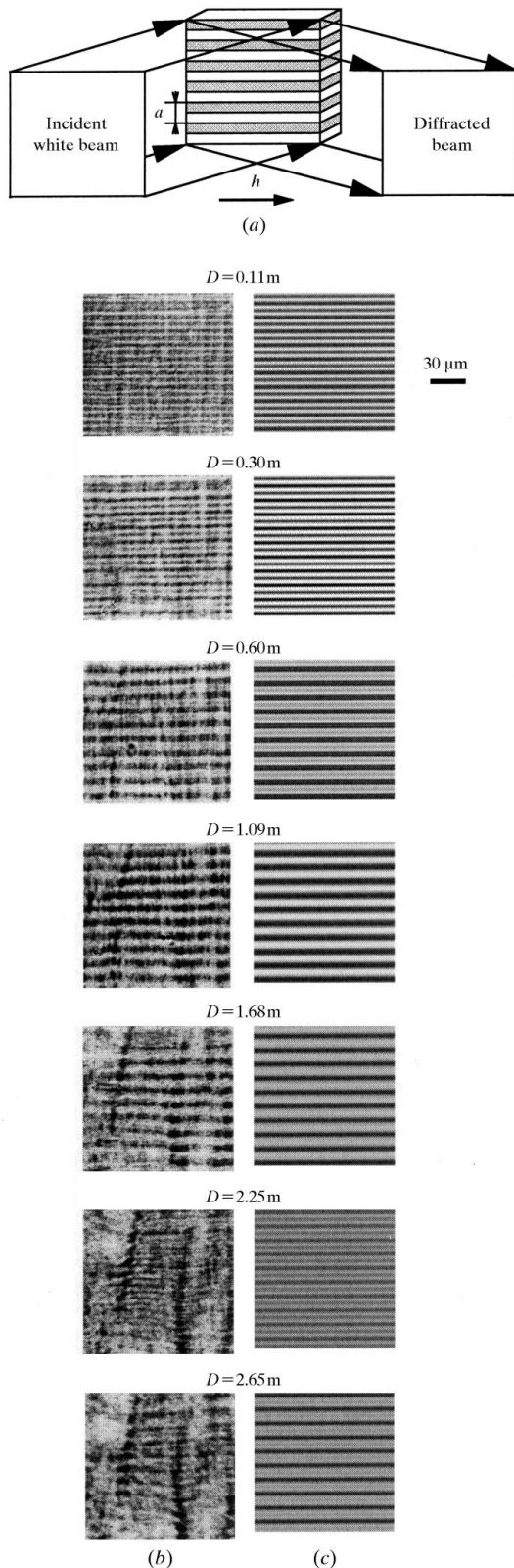
D = 1.68 m

D = 2.25 m

D = 2.65 m

(b) (c)

Figure 3
(a) Scheme of the white-beam experimental set-up for imaging ferroelectric domains in periodically poled crystals. (b) Experimental and (c) simulated images of a lithium niobate crystal (period = 14.8 μm, 006 reflection, E = 12.4 keV) for different sample-to-detector distances. The phase modulation used for the simulations is a periodic rectangular profile with a phase shift of 140°.

of the structure factor of the Bragg reflection used, the distribution of the phase in a plane perpendicular to the diffracted direction near the exit face of the poled specimen will be alternately $\varphi_{\mathbf{h}}$, the phase of the structure factor in one domain, and $\varphi_{-\mathbf{h}}$, resulting from crystal inversion, or equivalently reversal of the diffraction vector $\mathbf{h}$. Just as in the case of phase radiography, but now in the diffracted beam, the difference in phase will therefore induce, at a finite distance from the specimen, Fresnel diffraction fringes, *i.e.* an intensity modulation, from which the difference $\varphi_{\mathbf{h}} - \varphi_{-\mathbf{h}}$ can be directly extracted (Rejmán-ková-Pernot *et al.*, 1998). Fig. 3 illustrates the experiment and simulations which allow extraction of the phase shift for the 006 reflection of an LiNbO$_3$ crystal. This approach, although clearly restricted in its range of application, provides quantitative information on the relative atomic displacements in the two domains.

5. Conclusions

The use of the coherence properties of the beams delivered by the new synchrotron radiation sources is pushing up dramatically, and in many respects well beyond the expectations, the possibilities and applications of X-ray imaging. These techniques benefit from the development of adapted detectors, like the CCD FRELON camera (Labiche *et al.*, 1996) and scintillators, as well as from instrumental developments in X-ray optics, which could allow the magnification of the images (Lagomarsino *et al.*, 1997; Lengeler *et al.*, 1999). However, even in the present state of the art they are invaluable tools for solving a large variety of scientific and industrial problems. Phase imaging and tomography are, when using a modern synchrotron radiation source, instrumentally easy: their applications are a rapidly increasing field which includes biological and materials science topics. Diffraction topography remains a unique tool for characterizing single crystals and for investigating many crystal physics phenomena (creation of defects, domains, phase transitions, vibrations *etc.*). Its scope is enlarged to unexpected topics by the use of coherent beams.

References

Authier, A. (1996). *X-ray and Neutron Dynamical Diffraction: Theory and Applications*, edited by A. Authier, S. Lagomarsino & B. K. Tanner, pp. 1–31. New York: Plenum Press.
Baruchel, J. (1996). *X-ray and Neutron Dynamical Diffraction: Theory and Applications*, edited by A. Authier, S. Lagomarsino & B. K. Tanner, pp. 199–210. New York: Plenum Press.
Bonse, U., Beckmann, F., Busch, F. & Günnewig, O. (1998). *X-ray Microscopy and Spectromicroscopy*, edited by J. Thieme, G. Schmahl, E. Umbach & D. Rudolph. Berlin-Heidelberg: Springer-Verlag.
Bonse, U. & Hart, M. (1965). *Appl. Phys. Lett.* **7**, 99.
Buffière, J.-Y., Maire, E., Cloetens, P., Lormand, G. & Fougères, R. (1999). *Acta Mater.* **47**, 1613–1625.

Chapman, D., Thomlinson, W., Zhong, Z., Johnston, R. E., Pisano, E., Washburn, D., Sayers, D. & Segre, C. (1998). *Synchrotron Rad. News*, **11**(2), 4–11.

Cloetens, P., Barrett, R., Baruchel, J., Guigay, J. P. & Schlenker, M. (1996). *J. Phys. D*, **29**, 133–146.

Cloetens, P., Guigay, J. P., De Martino, C., Baruchel, J. & Schlenker, M. (1997). *Opt. Lett.* **22**, 1059–1061.

Cloetens, P., Ludwig, W., Baruchel, J., Guigay, J. P., Rejmánková-Pernot, P., Salomé, M., Schlenker, M., Buffière, J.-Y., Maire, E. & Peix, G. (1999). *J. Phys. D*, **32**, A145–151.

Cloetens, P., Ludwig, W., Baruchel, J., Van Dyck, D., Van Landuyt, J., Guigay, J. P. & Schlenker, M. (1999). *Appl. Phys. Lett.* **75**, 2912–2914.

Cloetens, P., Pateyron-Salomé, M., Buffière, J.-Y., Peix, G., Baruchel, J., Peyrin, F. & Schlenker, M. (1997). *J. Appl. Phys.* **81**, 5878–5886.

Coene, W., Janssen, G., Op de Beeck, M. & Van Dyck, D. (1992). *Phys. Rev. Lett.* **69**, 3743–3746.

Davis, T. J., Gao, D., Gureyev, T. E., Stevenson, A. W. & Wilkins, S. W. (1995). *Nature (London)*, **373**, 595–598.

Espeso, J., Cloetens, P., Baruchel, J., Härtwig, J., Mairs, T., Biasci, J. C., Marot, G., Salomé, M. & Schlenker, M. (1998). *J. Synchrotron Rad.* **5**, 1243–1249.

Förster, E., Goetz, K. & Zaumseil, P. (1980). *Krist. Technik.* **1**, 937–945.

Hu, Z. H., Thomas, P. A., Snigirev, A., Snigireva, I., Souvorov, A., Smith, P. G. R., Ross, G. W. & Teat, S. (1998). *Nature (London)*, **392**, 690–695.

Ingal, V. N. & Beliaevskaya, E. A. (1995). *J. Phys. D*, **28**, 2314–2317.

Kuznetsov, S., Snigireva, I., Souvorov, A. & Snigirev, A. (1999). *Phys. Status Solidi A*, **172**, 3–13.

Labiche, J. C., Segura-Puchades, J., Van Brussel, D. & Moy, J. P. (1996). *ESRF Newsl.* **25**, 41–43.

Lagomarsino, S., Cedola, A., Cloetens, P., Di Fonzo, S., Jark, W., Soullié, G. & Riekel, C. (1997). *Appl. Phys. Lett.* **71**, 2557–2559.

Lang, A. R., Kowalski, G., Makepeace, A. P., Moore, M. & Clackson, S. G. (1987). *J. Phys. D*, **20**, 541–544.

Lang, A. R. & Makepeace, A. P. (1999). *J. Synchrotron Rad.* **6**, 59–61.

Lengeler, B., Schroer, C. G., Richwin, M., Tümmler, J., Drakopoulos, M., Snigirev, A. & Snigireva, I. (1999). *J. Phys. D*, **74**, 3924–3926.

Mancini, L., Janot, C., Loreto, L., Farinato, R., Gastaldi, J. & Baruchel, J. (1998). *Philos. Mag. Lett.* **78**, 159–167.

Mancini, L., Reinier, E., Cloetens, P., Gastaldi, J., Härtwig, J., Schlenker, M. & Baruchel, J. (1998). *Philos. Mag. A*, **78**, 1175–1194.

Momose, A., Takeda, T. & Itai, Y. (1995). *Rev. Sci. Instrum.* **66**, 1434–1436.

Rejmánková-Pernot, P., Cloetens, P., Baruchel, J., Guigay, J. P. & Moretti, P. (1998). *Phys. Rev. Lett.* **81**, 3435–3438.

Snigirev, A., Snigireva, I., Kohn, V., Kuznetsov, S. & Schelokov, I. (1995). *Rev. Sci. Instrum.* **66**, 5486–5492.

Somenkov, V. A., Tkalich, A. K. & Shil'shtein, S. Sh. (1991). *Sov. Phys. Tech. Phys.* **361**, 1309–1311.

Spanne, P., Raven, C., Snigireva, I. & Snigirev, A. (1999). *Phys. Med. Biol.* **44**, 1–9.

Talbot, H. F. (1836). *Philos. Mag.* **9**, 401–407.

Tanner, B. K., Keir, A. M., Möck, P., Whitehouse, C. R., Lacey, G., Johnson, A. D., Smith, G. W. & Clark, G. F. (1998). *Proc. SPIE*, **3448**, 100–107.

Wilkins, S. W., Gureyev, T. E., Gao, D., Pogany, A. & Stevenson, A. W. (1996). *Nature (London)*, **384**, 335–338.